Airborne Lidar measurements and model simulations of tides, waves, and surface slope at the mouth of the Columbia River

R. Branch, A. Horner-Devine, C. Akan, C. Chickadel, G. Farquharson, *Senior Member, IEEE,*, A. Hudson, S. Talke, J. Thomson, and A. Jessup.

***Abstract*—Airborne Lidar measurements and model simulations are used to investigate the temporal and spatial variability of the water surface elevation at the mouth of the Columbia River. A series of 15 km transects repeated in 2-3 hour flights over a two week period resolve processes at a range of scales that are important to the dynamics of the river mouth region, including tides, surface slope, surface gravity waves, and wave-setup. Water surface elevations agree well with a nearby tide gauge, with an average difference of 0.01 m and an RMSE of 0.39 m. Significant wave heights derived from the Lidar measurements agree well with *in-situ* wave drifter measurements, and are observed to react to both bathymetry and spatial/temporal variations in currents, increasing up to 228 percent on large ebb tides. Surface slopes varied from 2.7×10^{-5} to -2.6×10^{-5} over the course of a typical tide to as large as 6.3×10^{-5} to -4.8×10^{-5} during a larger tide. The magnitude of the setup and setdown due to wave height amplification during ebb tide was estimated to be 4×10^{-6}. These observations demonstrate that many of the key dynamical variables at river mouths can be determined from airborne remote sensing measurements of water surface elevation and suggest that forthcoming altimetry products, such as those from the Surface Water Ocean Topography altimeter, may be able to provide new insight on monitoring in these complex regions.**

***Keywords*—Altimetry, tides, surface waves, rivers.**

I. Introduction

River discharge into the ocean influences coastal stratification and coastal currents [1], carries sediments and nutrients into the ocean [2], and, considered globally, forms an incompletely known portion of the global water mass balance and sea-level budget. Since river slope is related to discharge, remotely sensing river and coastal water surface elevations has become an active area of research [3], particularly due to recent and planned advances in the resolution and coverage of satellite altimeters, including the upcoming launch of the SWOT (Surface Water Ocean Topography) altimeter which will be used to investigate sea level variability in the coastal zone [4]. The SWOT altimeter, which will measure with a swath resolution of $<$ 60 m, slope accuracy of 1.7 cm/km for water areas $>$ 1 km^2, vertical accuracy $<$ 25 cm, and return period of 20.86 days [5], is designed to measure water levels in regions of little or no data. A primary SWOT science objective is to calculate river discharge from measurements of water surface elevation [6]. The presence of tides, however, greatly complicates measurements of river flow near the mouth due to non-linear tide-current interaction, the compensation flow for Stokes drift, and other factors [7] [8]. Hence, while a slope/discharge technique has been used with remote sensing data before, it is limited to regions far from the mouth [9]. Such measurements miss the effect of coastal tributaries and other factors such as evaporation or water withdrawal which can significantly influence the water mass balance. To avoid these confounding factors, one would ideally measure discharge at the river mouth, using the water level slope after correcting for the influence of tides (e.g., method of [10]).

In this paper, we present the first airborne Lidar measurements of sea surface elevation at a river mouth which we combine with a numerical model to investigate dynamical processes. The mouth of the Columbia River (MCR) is a critical dynamical region for navigation and connectivity between the ocean and the river environment. It is an energetic region subject to high river discharges, large waves, significant tides, and strong winds. This effort builds off the results of [10], who used airborne Lidar to measure river slope within the tidal river but did not measure at the river mouth where the complexity of the region introduces different processes such as wave amplification, that can influence the sea surface elevation and slope. Specifically, this research investigates the feasibility and challenges of measuring water levels and surface slopes at the river mouth in order to evaluate the potential for estimating coastal river discharge from remotely sensed data.

Airborne Lidar measures the distance between an airplane and the water surface using a laser time-of-flight ranging system, and corrects for plane movement using an inertial navigation system. The airplane moves quickly (40 m/s) sampling a 15 km stretch of river in 5-10 minutes. Each 15 km transect is a snapshot of the conditions, assuming that currents and waves are stationary over that time period. The rapidly sampled Lidar measurements provide high spatial resolution sufficient for resolving surface waves. This enables us to assess the effects of small scale variability such as wave setup that might not be detectable by spaceborne sensors. Several Lidar transects can be combined to form a swath of the conditions over a half hour period. The combined data provides a unique

R. Branch is with the Department of Civil and Environmental Engineering, University of Washington, Seattle, WA, 98195 USA e-mail: (rbranch@uw.edu).

A. Horner-Devine, C. Chickadel, G. Farquharson, J. Thomson and A. Jessup are with the University of Washington. C. Akan is with the University of North Florida. A. Hudson and S. Talke are with Portland State University.

Manuscript received Oct. 24th, 2017; revised Dec. 20th, 2017.

platform to simultaneously measure waves and tides rather than only tides [10] or waves [11].

Wave height amplification due to wave-current interactions is a well known navigational hazard at the MCR, but is difficult to measure *in-situ* due to dangerous, spatially and temporally variable, and highly energetic conditions. Moored [12] and drifting buoys [13] have measured significant wave heights amplified by a factor of three near the mouth compared with locations offshore during ebb tide, but the spatial and temporal effects of tides on waves have not been empirically quantified. Numerical modeling studies predicted that wave-current interactions cause an increase in wave height of almost 200% during ebb [14][15]. Since wave amplification can produce patterns of setup and setdown, such spatial variations may influence remotely sensed water levels and thus affect estimates of tidal slope or river discharge from the measurements.

Surface elevation changes with the tide have been predicted by numerical models at the MCR in order to study the vertical current structure [14], wave-current interactions [15], plume spreading [16], and tidal salt transport mechanisms [17]. The models showed strong qualitative agreement with in-situ tidal gauges however they did not study the surface elevation for the purposes of quantifying the surface slope. One goal of this research is to determine if the slope changes caused by the tide can be measured remotely. If slope changes due to the tide can be quantified and removed from the elevation signal, then it may be possible to measure slope changes due to river discharge.

In this paper we use airborne Lidar data and a numerical model to study the water surface elevation, waves, and surface slope at the mouth of a river. In the Methods section we describe how the Lidar data were acquired and how the physical parameters such as significant wave height and surface slope were calculated from the data. We also describe the numerical model and how it was run for the same time period that the Lidar data were acquired. In the Results section we verify that the Lidar correctly measures water surface elevation, waves, and surface slope by comparing our results with tide gauges, drifting wave buoys, and the numerical model outputs. In the Discussion section we outline possible sources of measurement error and natural variability that cause differences between the Lidar measurements and *in-situ* measurements or model predictions. In the Conclusions section we summarize the success of the airborne Lidar at studying the physical processes at the mouth of the Columbia River and discuss directions for future research.

II. METHODS

A. Study Site

The Columbia River discharges into the Pacific Ocean on the west coast of North America, on the border between Oregon and Washington state. Tide, wave, and discharge conditions are monitored continuously near the MCR by NOAA (National Oceanographic and Atmospheric Administration), NDBC (National Data Buoy Center), and the USGS (United States Geological Survey) due to its navigational and ecosystem importance in the region. We compare Lidar measurements of tides with tidal levels measured by NOAA at the Hammond station (station 9439011, river kilometer 15 from the mouth) and waves with offshore wave measurements at the NDBC buoy 46029 (37 km offshore) (Fig. 1b). River discharge was measured by the USGS at the Beaver Army Terminal (river kilometer 86, Fig. 1b), where 97% of the total freshwater discharged into the ocean is measured [18], [19].

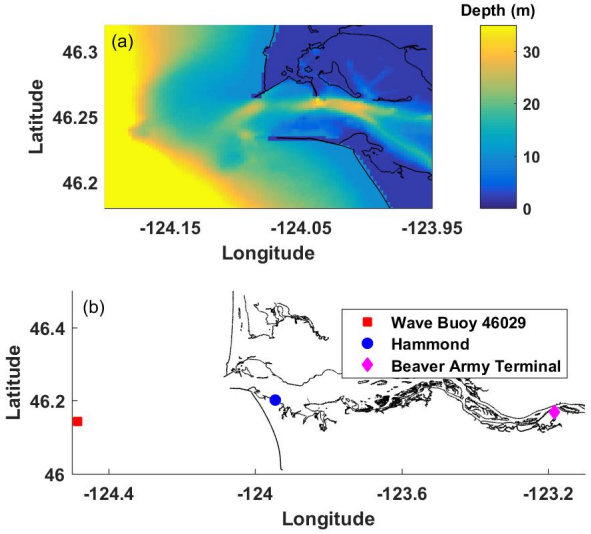

Figure 1. Study site at the MCR. (a) The bathymetry shows the influence of the three jetties and channel dredging. (b) Locations of the wave buoy 46029, tidal station at Hammond, and discharge measurement at Beaver Army Terminal.

The bathymetry at the MCR is complex due in part to the influence of maintenance dredging and three jetties which channelize flow and promote ebb currents of up to 3 m/s [14]. The depth varies from 15-30 m between the estuary and the ocean (Fig. 1a). A shallow area just east of the jetties is called the ”inner bar” and west of the jetties to longitude -124.17 is called the ”outer bar”, though no shoals are exposed during low tide [12].

B. Lidar instrumentation and experimental conditions

Airborne Lidar data were collected with a Riegl LD90-3800EHS-FLP instrument flown on a Cessna 172SP. The Lidar measures the distance between the plane and the water uncorrected for plane altitude or elevation. Pitch and roll accuracy was less than 0.01 degrees and heading accuracy was less than 0.025 degrees. The GPS was receiving Omnistar HP position correction information via satellite, which reduced 95% of the vertical position errors to less than 10 cm, based on the manufacturer’s assessment. The IMU had a variable time offset and possible drift with respect to the Lidar clock which was corrected by using a method based on a Taylor’s series expansion [10].

Data were analyzed from 26 flights flown on 20 days from May to September 2013, with most of the data collection from May 26th through June 10th. The May through June

experiment spanned wave conditions with significant wave heights of 0.67 to 3.51 m, tidal heights of -1.88 to 1.71 m, and river discharge of 7,895 to 10,902 m^3/s (Fig. 2). These are all within the range of typical summer values at the MCR. The plane could only fly during daylight, which meant that no flight sampled an entire tidal cycle (Fig. 2a). Each flight flew multiple transects in and out of the mouth of the river. An example flight track from May 26th that included eight transects is shown in Figure 3a. Each transect was approximately 15 kilometers long and took the airplane 5-10 minutes to complete.

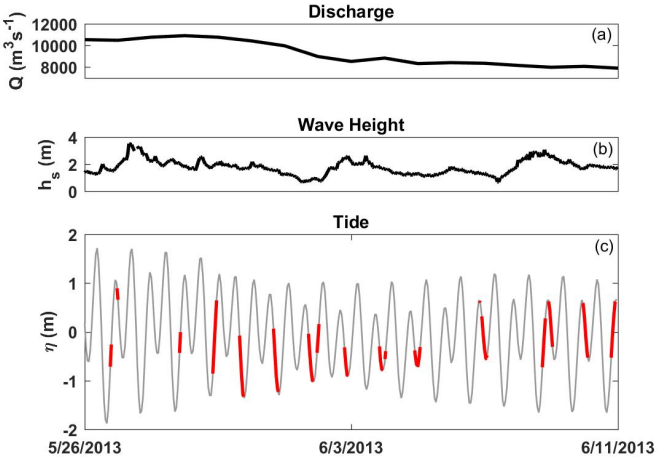

Figure 2. a) Discharge, Q, measured at Beaver Army Terminal, b) wave height, h_s, measured by buoy 46029, and c) tidal water surface elevation, η, measured at Hammond during the main data collection period. Red lines indicate Lidar flight times.

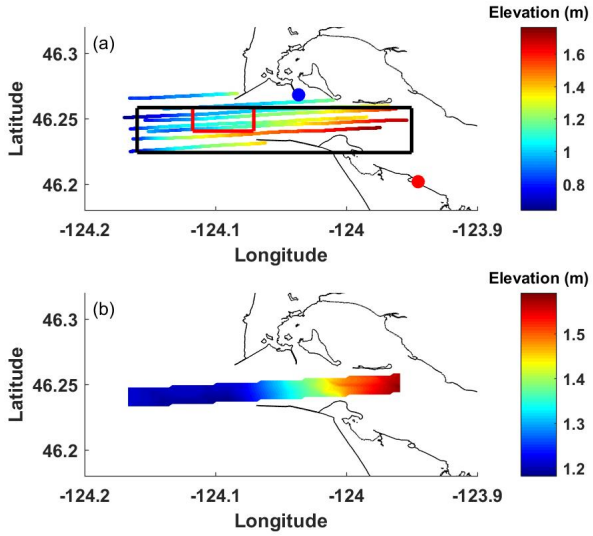

Figure 3. (a) Water surface elevation measured by Lidar during eight flight transects on May 26th. Location of the focus area (red box) where Lidar water surface elevation measurements were compared with concurrent in situ data collected at the NOAA Hammond tidal gauge (red dot) and historical data collected at the NOAA Jetty A tidal gauge (blue dot). Location of the Lidar water surface elevation measurements (black box) used in the surface slope calculations. (b) Model water surface elevation values used to calculate a model predicted surface slope.

C. Lidar measurement of elevation

Water surface elevation, η, is calculated with respect to mean sea level (MSL) using the Lidar, GPS, and the IMU. Three geometric corrections are applied to the raw Lidar distance measurement to obtain a corrected distance L. First, the distance between the Lidar and the IMU is added to give a new vector. This vector is then multiplied by a rotation matrix to obtain a vector whose z component is the vertical distance between the IMU and the water. The vertical distance between the IMU and GPS is then added to that to obtain a vertical distance between the GPS and a point on the ellipsoid with the latitude and longitude coordinates output by the GPS. The GPS also outputs its height, h, above the WGS-84 ellipsoid. The difference between the ellipsoid and MSL (as approximated by the EGM96 geoid) at a particular latitude and longitude is called the undulation, N. The undulation varies by location and depends upon the choice of geoid. The elevation, η, of the water surface above or below MSL is then given as

$$\eta = h - L - N. \tag{1}$$

This elevation is an orthometric height which can be compared with tidal gauges. The elevation values were divided into flight transects and data were discarded on either end of the transects where the airplane was turning. Observations over land and clouds were also discarded.

Elevation values within the red box shown in Figure 3a were averaged spatially and temporally during each ten minute flight transect and compared with the closest concurrent tidal measurements at Hammond. The ten minute sampling time is

very small compared to tidal timescales and the sampling time required for a similar measurement from a boat. We calculated the M2 amplitude by harmonic analysis [20] of Lidar elevation data, concurrent Hammond data (NOAA station 9439011) and two months of hourly Jetty-A data from 1997 (NOAA Station 9440572). A reduced constituent set consisting of M2 and K1 constituents was applied due to the shortness of the record.

D. Lidar measurement of waves

The Lidar sampled at 3 kHz, which corresponds to a 0.5-1.0 m footprint and provides good resolution of the water surface elevation variation due to waves (Fig. 4). To isolate waves in the Lidar data a 5th order polynomial fit was subtracted from the raw elevation data. This removed any low frequency noise due to inaccurate plane motion corrections or timing errors. From this detrended data, significant wave height, h_s, was calculated as four times the standard deviation [21] of 60,000 elevation measurements which roughly corresponded to 1 km of flight track. Wavelength was calculated as the inverse of the peak frequency of a wavenumber spectrum of a 2 km section of water surface elevation data.

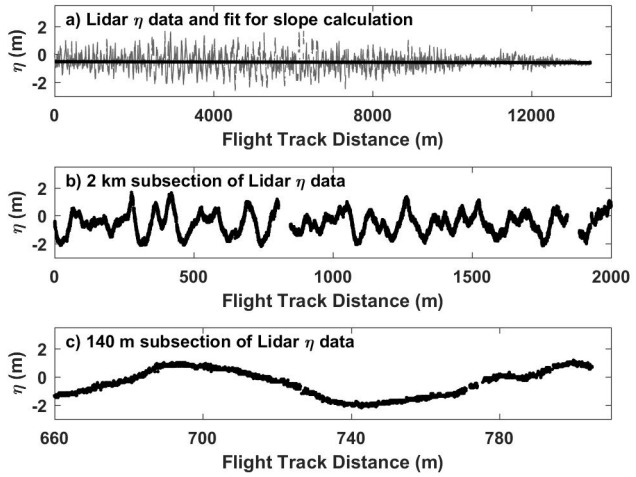

Figure 4. a) Example Lidar η data from one transect. The linear fit is used for the slope calculation. The airplane was flying west to east so a flight track distance of 0 is west of the mouth. b) Example of Lidar η data resolving several waves on a 2 km subsection of the transect. c) Example of Lidar η data showing an individual wave on a 140 m subsection of the transect.

Significant wave heights calculated from the Lidar data were compared with significant wave heights measured by offshore buoy 46029 (Fig. 1) to compute the wave amplification. Wave amplification is defined as

$$\beta = \frac{h_s}{h_{s0}} \tag{2}$$

where h_s is the local significant wave height and h_{s0} is the offshore significant wave height.

E. Lidar measurement of surface slope

The surface slope of each transect was calculated from a linear fit to all surface elevation data located within the black box of Figure 3 a). Transects were excluded if they had fewer than 100,000 points in the box or if more than half of their points in the box were missing due to land or clouds.

Surface slopes can be influenced by changes in wave heights (due to shoaling, breaking, or wave current interactions), which cause gradients in the radiation stress, S_{xx}, that depress or elevate the local mean sea level. Radiation stress is a function of the wavenumber, k, depth, d, and energy, $E = \frac{1}{16}\rho g h_s^2$. As the waves are amplified, h_s increases, subsequently increasing their energy and the radiation stress according to

$$S_{xx} = E\left(\frac{2kd}{\sinh 2kd} + \frac{1}{2}\right). \tag{3}$$

Gradients in radiation stress causes a change in surface slope, $\frac{\partial \eta}{\partial X}$, given by

$$\frac{dS_{xx}}{dX} = -\rho g d \frac{\partial \eta}{\partial X}. \tag{4}$$

F. Datasets for validation and comparison

Lidar significant wave heights were validated with measurements made by SWIFT (Surface Wave Instrument Float with Tracking) drifting wave buoys [22]. The SWIFTs estimate significant wave height using spectra of ten minute bursts of GPS Doppler velocities as a measure of wave orbital motion [23]. They were deployed on five of the same days as the Lidar, and were released east of the jetties on ebb tide to drift out through the mouth. On some days they drifted back towards the mouth on flood tide but on other days they drifted north or south of the mouth with the prevailing current.

Lidar measurements of elevation, surface slope, and wave amplification were compared with numerical simulations made using the COAWST modeling system [24], in which the 3D ocean circulation model (ROMS: Regional Ocean Modeling System) is two-way coupled to the phase-averaged wave propagation model (SWAN: Simulating WAves Nearshore) [15]. The model uses a 3-level nested grid with the highest resolution grid having a horizontal resolution of 200 m. Model predictions were made every half hour over the measurement period. Model predicted surface slope was calculated from a linear fit to model elevation values versus track distance. The location of the model elevation values used in the calculation is shown in Fig. 3b). The gridded model latitudes and longitudes were first converted into universal transverse Mercator (UTM) coordinates and then into a track distance array.

Lidar measurements of tidal elevation were compared with measurements made by NOAA at the Hammond tidal gauge (Fig. 3a).

III. Results

A. Elevation

The Lidar elevations measured in the focus area at the MCR (Figure 3a; red box) were averaged for 260 flight transects and compared with the tidal levels measured at Hammond. The

Lidar elevations agreed with the tidal elevation (Fig. 5) with an average difference of 0.01 m (Lidar > tidal) and RMSE of 0.39 m. The maximum tidal level measured by the Lidar was 1.0 m above MSL and the minimum was 1.96 m below MSL. The average difference is smaller than the datum uncertainty for the NOAA tide datum at the Columbia River which is 0.23 m [25]. The RMSE is similar in magnitude to previously published values of a shorter experiment comparing Lidar elevations to seven tidal gauges upriver of the mouth but the average difference is much smaller [10]. The previous study used the same airborne Lidar system and found an average difference of 0.48 m with an RMSE of 0.41 m. The larger difference at the upriver locations may be due to a slightly different plane motion correction algorithm used in that study or larger datum uncertainties at the upriver location. The RMSE may be due to measurement errors or natural variability, which is discussed in more detail in section IV.

Harmonic analysis of the Lidar elevation data gave an M2 tidal amplitude of 0.83 +/- 0.16 m, which is in good agreement with the M2 amplitude of 0.86 +/- 0.01 m calculated from a two month long historical dataset from Jetty A (Fig. 3a). The Hammond data from the same time period gives an M2 amplitude of 0.93 +/- 0.00 m. This is larger than the Lidar and historical data at Jetty A, which suggests that there is amplification of the tide between Jetty A and Hammond.

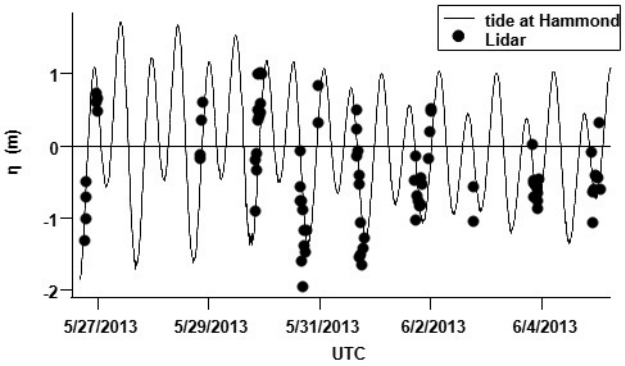

Figure 5. Water surface elevation from the tide gauge at Hammond and Lidar measurements inside the red box shown in Figure 3a.

B. Waves

1) Comparison with in-situ measurements:

Lidar h_s measurements were compared with the SWIFT measurement that was taken closest in space to the Lidar transect. Due to logistical constraints of the sampling, Lidar transects and SWIFT drifts were chosen with as much, but no greater than 14 hours time separation. In all, 579 h_s values were compared and agreed well; the mean difference was 0.27 m (SWIFTs > Lidar) and the RMSE was 0.62 m. The maximum h_s measured by the Lidar during the comparison period was 2.25 m and the minimum was 0.55 m.

An example comparison of Lidar and SWIFT wave heights is shown in Figure 6 from May 26th as the SWIFTs drifted through the river mouth and the Lidar flew overhead. Both

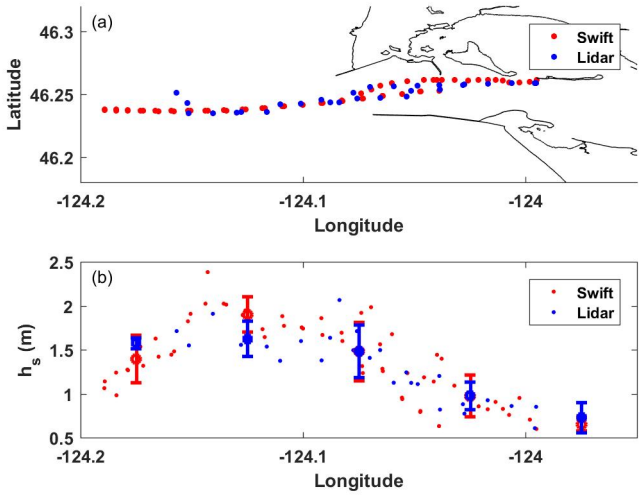

Figure 6. (a) Location and (b) magnitude of SWIFT and Lidar h_s measurements from May 26th.

the Lidar and SWIFTs measured smaller waves (h_s = 0.7 m) inside the mouth east of longitude -124 and larger waves (h_s = 1.48 m) at the mouth near longitude -124.07. Data from both platforms shows that wave heights increased further out to sea near longitude -124.125 and then decreased west of longitude -124.15.

2) Amplification due to wave-current interactions:

Wave amplification occurs at river mouths due to the shoaling and refractive focusing of waves in shallower water and / or the action of surface currents opposing the wave propagation direction. Wave amplification was observed with the SWIFTs and Lidar, and predicted by the numerical model during ebb tides. The strongest wave amplification observed by the Lidar occurred on an ebb tide on May 31st (Fig. 7 a, c, e). Wave amplification derived from the Lidar, β_{Lidar}, was calculated using (2) with h_s measured by the Lidar referenced to h_{s0} measured by wave buoy 46029 offshore. The Lidar flight began around 16:00 and showed amplification close to the mouth. As the tide continued to ebb, the region of wave amplification extended further out into the ocean and became stronger near the mouth. The flight continued until 19:00 when the amplification was still present but had decreased in magnitude.

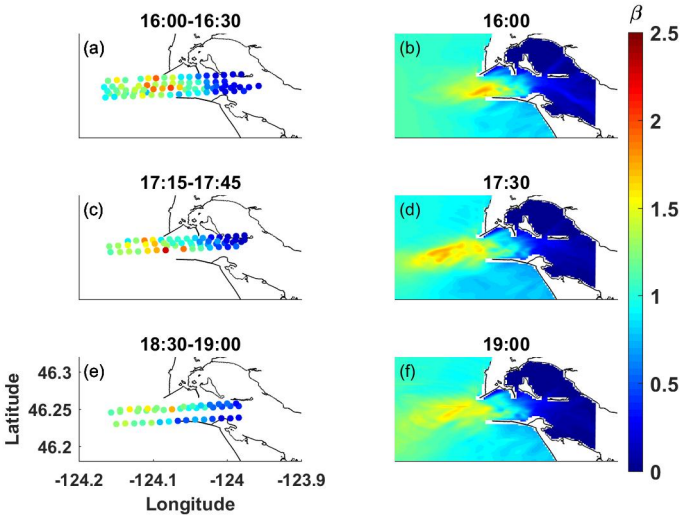

Figure 7. Maps of wave amplification measured by the Lidar (a, c, e) and calculated by the model (b, d, f) during an ebb tide on May 31st

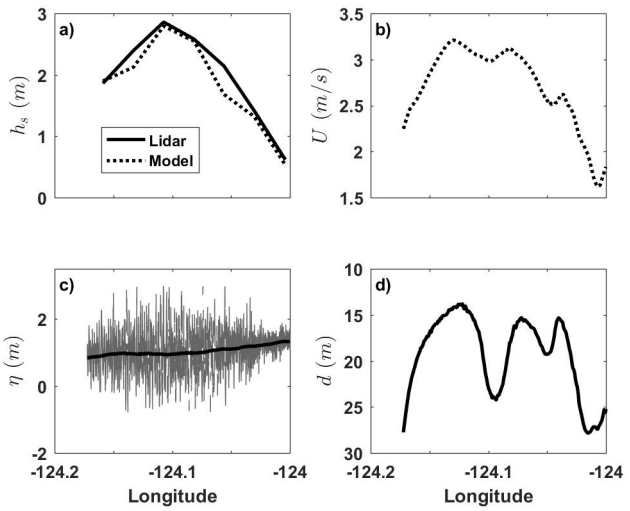

Figure 8. a) Significant wave heights, h_s, b) westward current velocity, U, c) surface elevation, η, and d) water depth, d, plotted vs. longitude. Data were acquired during ebb tide on May 31st along the 16:14-16:19 flight transect.

The modeled wave amplification β_{model} was calculated using (2) with h_s calculated by the model and referenced to h_{s0} measured by wave buoy 46029 offshore. The model agreed with the Lidar, showing wave amplification beginning near the mouth at 16:00, spreading further into the ocean by 17:30, and decreasing in magnitude but not extent by 19:00 (Fig. 7 b, d, f).

Wave amplification at the MCR occurs as the waves propagate shoreward into shallower water and into a strong opposing ebb current. We further investigate the observed amplification by analyzing the current, significant wave heights, and depth along a single transect of the May 31 flight. This one-dimensional analysis obscures the distinction between shoaling and refractive focusing over horizontal gradients in the bathymetry and the currents. Both are important processes at river mouths; this analysis quantifies the net combined effect of these processes. The westward current peaks between longitudes -124.1 and -124.2, which is also where the significant wave heights peak (Fig. 8 a b). The depth is shallower where this peak occurs (Fig. 8 d), but we do not observe a response in wave height to every change in bathymetry east of this (Fig. 8 a d). Most of the waves on the flight transect shown in Figure 8 are intermediate waves ($\frac{d}{\lambda} < 0.5$), meaning that their wave heights are affected by the bottom and will increase as the depth decreases. As they propagate further east of -124.03, they encounter deeper water and lower opposing velocities, leading to decreased wave heights. Reductions in wave heights also are caused by wave breaking just west of -124.03 [26].

Analysis of seven transects from the flight shown in Figure 7 confirms that the wave amplification is dependent upon both current velocity and depth (Fig. 9). Wave amplification increases as the current increases and is stronger when η is below mean sea level due to shoaling. These results agree with the findings of [12] who came to the conclusion that wave-current interactions are the dominant physical mechanism governing wave amplification with bathymetric effects being of secondary importance. The related processes of wave breaking, refraction, and diffraction are not separated here, but likely all affect wave amplification. Although wave amplification is a complicated process at the MCR, Figure 9 demonstrates that it can be estimated from remotely sensed data. Due to the dominant dependence on the opposing velocity, this presents a possible opportunity to estimate the river velocity from the wave amplification and water surface elevation measurements.

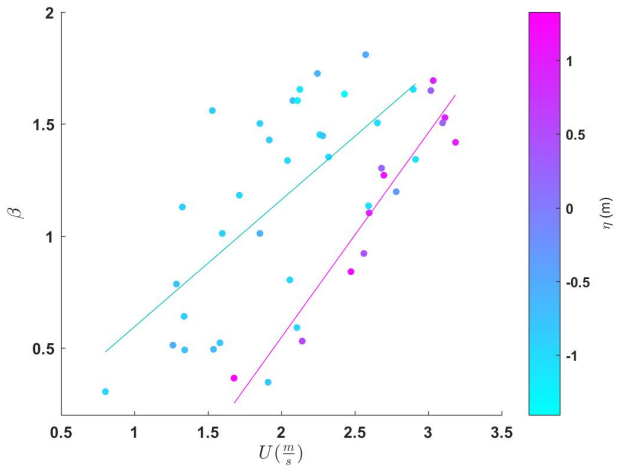

Figure 9. Wave amplification, β, as a function of westward current velocity, U, and water surface elevation, η. Linear fits are to all points where the water surface is above (magenta) and below (turquoise) mean sea level (MSL). MSL corresponds to $\eta = 0$.

C. Surface slope

The surface slope was calculated for each Lidar transect and compared with slope estimated from the numerical model output. The minimum and maximum measured slopes were -4.8×10^{-5} and 6.3×10^{-5}, corresponding to flood and ebb tides, respectively. Here, positive slopes are associated with higher water east of the mouth. Four Lidar transects are shown in Figure 10 (a, b, c, d) during different tidal phases. The slope is negative on flood tide and positive on ebb. There is a kink in the ebb tide slope near -124.015 when η is below MSL (0) (Fig. 10 c). The model predictions agree with this pattern and are plotted for an entire tidal cycle (10 e, f, g, h). The model transects show a progression from negative slope on flood increasing to zero at high tide (Fig. 10 e), increasing to a positive slope with a kink below MSL on ebb (Fig. 10 f, g), and then decreasing from zero to a negative slope on ebb again (Fig. 10 h).

The slopes calculated from the linear fits of the Lidar transect data were compared with the model slopes extracted at the same times. The average difference was 8.1×10^{-6} and the RMS of the difference was 1.9×10^{-5} with the average Lidar slope greater than the average model slope. A linear fit of the Lidar slopes vs the model slopes gave an r^2 value of 0.39 (Fig. 11 a). The differences between the Lidar and model slopes could be due to Lidar measurement errors or natural variability not resolved by the model. Sources of error and natural variability are discussed in section IV.

In order to investigate the Lidar and the model slopes in more detail, the slope of each Lidar transect was plotted versus time from high tide, averaged in half hour bins from high tide, and plotted with the half hour averages of the corresponding model slopes (Fig. 11 b). Both Lidar and model slopes show a sinusoidal pattern, with positive slopes during ebb and negative slopes during flood. After high tide the slope increases from zero as the tide ebbs and reaches its maximum slope two hours after high tide. It then continues to decrease during ebb until reaching zero at the end of ebb tide. As the tide changes to flood, the slope becomes negative and decreases to the minimum (negative) slope eleven hours after high tide. It then increases back to zero slope as high tide is approached. The Lidar measurements resolved the tidal variations and the model predictions agreed with the Lidar within the error bars for most of the tidal cycle (Fig 11 b). The tidal variation is strong in the average signal but the slope of each individual transect differs from the average due to the size of the tide and other factors such as measurement error, discharge, intermediate scale flow structures, upwelling, and wave setup.

D. Slope changes from wave-current interactions

Slope changes from wave-current interactions were investigated by examining gradients in energy and radiation stress in the cross-shore direction. Energy and radiation stress are related to significant wave height and will increase in areas where an opposing current amplifies the wave heights. Energy, calculated from Lidar and model h_s values, varies along the flight transect plotted in Figure 12 a). The energy peaks around longitude -124.1 where the significant wave height also had a peak (Fig. 8a). The wavelength, λ, varies along the flight transect (Fig. 12 b) but was modeled as lower than the Lidar measured for most of the track. The radiation stress also had a peak near longitude -124.1 and was lower in the model predictions due to the differing wavelengths. The surface slope due to the radiation stress divergence, $\frac{\partial \eta}{\partial X} waves$, changes from negative to positive over the length of the transect (Fig. 12 d). It is important to note that the estimates of the surface slope due to radiation stress gradients are an order of magnitude smaller than the measured surface slope. This suggests that the wave impact on surface slope is small compared with that due to tides.

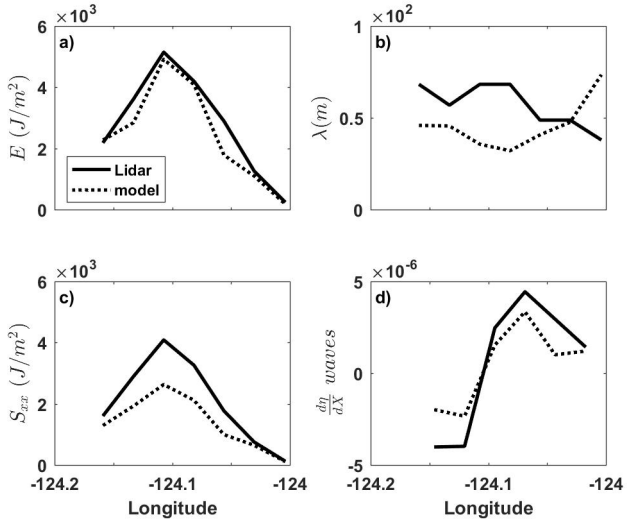

Figure 12. Wave energy, E, wavelength, λ, radiation stress, S_{xx}, and surface slope, $\frac{d\eta}{dX} waves$, vs. longitude along one flight transect. Data were acquired during ebb tide on May 31st along the 16:14-16:19 flight transect.

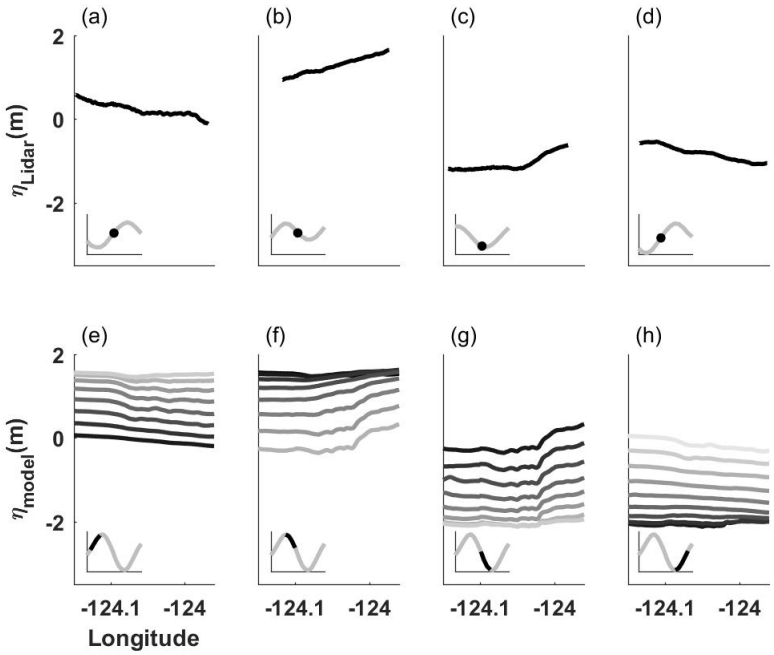

Figure 10. Lidar (a, b, c, d) and model (e, f, g, h) examples of the water surface elevation profiles during 4 phases of the tide. The Lidar profiles are from different tides because the Lidar never sampled a whole tidal cycle. The model profiles are all from the same tidal cycle. Time increments of the model profiles are 0.5 hours and time increases from the black line to the gray line.

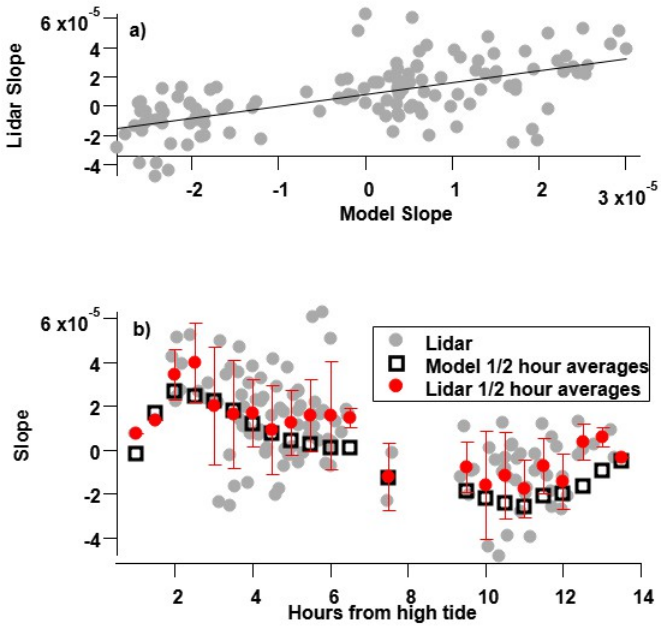

Figure 11. a) Slopes as measured with the Lidar and versus slopes calculated with the model. b) Slopes versus hours from high tide. Gray dots are Lidar slopes for each transect. Red dots are Lidar slope averages in half hour bins of hours from high tide with error bars of +/- 1 standard deviation. Black squares are model slope averages in half hour bins of hours from high tide.

IV. Discussion

The airborne Lidar measurements in this study resolved waves, water surface elevation, surface slope, and the changes of these parameters with the phase of the tide. A limitation of studying tidal changes using airborne Lidar is the daylight constraints of the flights. No complete tidal cycles were observed which meant changes in waves, water surface elevation, and surface slope with discharge were not resolved (Fig. 2). Complete tidal cycles would need to be observed under varying discharge conditions in order to separate out the tidal effects and determine whether discharge can be resolved. Waves were found to also influence the water surface elevation and surface slope, so a complete discharge study would require measurements of tidal cycles with similar offshore wave conditions.

The accuracy of the Lidar measurement of water surface elevation was determined by a comparison with the closest tidal gauge. The Lidar measurements compared so well with the tide gauge that the average difference of 0.01 m was smaller than the tide gauge datum uncertainty and the quoted Lidar instrument accuracy. The RMSE of 0.39 m was larger than the average difference and suggests errors which change in space or time rather than constant offset errors. Differences between the Lidar and tide gauge measurements may be due to measurement error or natural variability.

Measurement errors could cause a constant offset in the Lidar distance measurements or a time varying offset which depends on factors such as pitch and roll or location of the airplane. One example of a measurement error would be an incorrect distance between tide gauge MSL and the geoid

height. Uncertainty between the tide gauge MSL and the geoid can be on the order of 1 m [10] [25] and may vary by location. The uncertainty between the tide gauge MSL and the geoid could have been larger in the location of the previous upriver experiment, causing a higher average difference between the Lidar elevation and the tide gauge elevation.

Another possible source of measurement error is a time offset or drift between the IMU and the Lidar. This would impact the calculation of η in equation (1) because H and L would not be collocated. If H and L are not collocated and the airplane is not flying at a constant altitude, then an incorrect L value would be used in equation (1). This type of error is removed in the significant wave height calculation by the subtraction of the polynomial fit but it would have a large impact on the tidal elevation and slope measurements. An attempt was made to correct this possible error by using a method based on Taylor's series expansion [10].

Differences due to natural variability could be caused by the spatial separation between the tide gauge at Hammond and the location where the Lidar measured elevation. The water level is not the same at the mouth where the Lidar measured and at Hammond due to the propagation of the tidal wave. This difference varies with the phase of the tide. The level at Hammond would be higher than at the mouth during ebb and lower during flood. Harmonic analysis of the Hammond data and historical data at Jetty A showed different amplitudes of the M2 tide implying amplification of the tide between the two locations. Amplification of the tide would lead to non-linearly related water levels at the two locations.

In addition, the model output includes intermediate scale flow structures near the north jetty (Fig. 13a). These structures modulate the water elevation on spatial scales shorter than the Lidar transect and may also affect the tidal elevation and slope measurements. In particular, such structures are expected to display significantly more randomness than the tidal and discharge signals. While it is quite possible that the model captures these structures in a statistical sense, we do not expect that individual structures are well resolved. Since the water surface slopes on the edges of these structures are of a similar magnitude to the transect slopes, they may introduce a significant source of variability in the comparison between the Lidar measurements and the model slope outputs. Nonetheless, we observe evidence of such structures in both the Lidar and model, and they occasionally correspond in time. Figure 13b shows Lidar and model elevation data extracted for the Lidar flight transect shown in Figure 13a. The deviation from a more linear elevation profile (Figure 13b) appears to be associated with the presence of intermediate scale structures (Figure 13a), and is captured in the Lidar data. However, the variability east of the jetties differs and would lead to different computed slope values.

Surface slope has been previously studied with Lidar measurements upriver of where our measurements were made and found to be 1.8×10^{-5} [10]. We observe slopes with a similar magnitude during ebb tide but larger and smaller slopes were also measured due to the strong tidal signal near the mouth. The slope of 1.8×10^{-5} reported in [10] is a slope averaged over the tidal cycle from river kilometer 15 to river kilometer

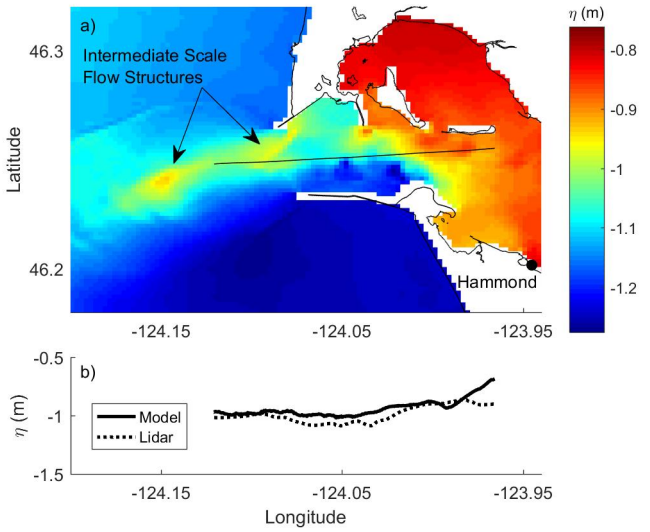

Figure 13. a) Model derived water surface elevations showing intermediate scale flow structures. Lidar flight transect location is shown as a black line. Black dot shows the location of the tidal gauge at Hammond. b) Model and Lidar water surface elevations along the flight transect.

75. They also reported a slope change near river kilometer 40 which they propose was due to changes in the river width. We would not expect our slope measurements to agree perfectly with those reported in [10] because the measurements were taken at different times and locations. Surface slope is expected to be dependent upon river width, phase of the tide, size of the tide, and discharge [27].

The magnitude of surface slopes measured at the river mouth with Lidar indicate that SWOT may be able to resolve flood and ebb tidal variations. Average values of the water surface slope determined from the Lidar measurements are approximately 3.5×10^{-5} and -1.8×10^{-5} at peak flood and peak ebb, respectively, and corresponding model estimates are approximately 2.2×10^{-5} and -2.2×10^{-5} (Figure 11b). SWOT's slope accuracy is projected to be 1.7×10^{-5} [5], suggesting that the measured and modeled peak tidal slopes are within a factor of one or two of the projected accuracy. This puts the SWOT accuracy on the threshold of the required accuracy; tidal peaks in slope may be resolvable in a phase averaged sense over many passes, but the observed variability is likely to obscure the tidal signal in individual passes. The surface slope could also be influenced by wave current interactions but our Lidar measurements show these changes would be too small to be observable by SWOT for the relatively mild conditions measured during our experiment.

The Lidar wave height amplification study presented here is the first of its kind at a river mouth. Wave height amplification at the MCR has been modeled and studied before with waverider buoys and radar but the spatial extent of amplification has not previously been measured [15][12][28]. The Lidar captured the magnitude and spatial extent of amplification during part of one ebb tide and the model agreed with those results. Lidar data were not acquired during the largest ebb

tide possible at the MCR so wave amplification may be even larger in magnitude and extent on a larger ebb tide. Wave amplification caused surface slope changes but those changes were an order of magnitude smaller than changes due to the tide. These wave-driven slope changes are only indirectly related to discharge and so they risk contaminating estimates of discharge from the surface slope at river mouths.

V. Conclusions

In this paper we successfully used airborne Lidar data and a numerical model to study tidal changes at the mouth of the Columbia River. When compared with *in-situ* and model estimates, agreement was good for the following Lidar measurements:

- water surface elevation
- water surface slope
- surface gravity waves

The success of the airborne Lidar at resolving tidal changes of the water surface elevation and surface slope implies that airborne Lidar can be used to detect the tidal cycle and amplitude remotely.

Tidal variation was also detected by the Lidar in wave changes. Wave measurements showed amplification as the river velocity increased on ebb tide. The ability of the Lidar to detect wave changes with velocity leads to the possibility of remote sensing of velocity and therefore discharge as velocity increases with discharge.

Future research will be conducted to determine how waves, water surface elevation, and surface slope change with river discharge at river mouths. Discharge is often related to surface slope by Manning's equation in locations without tidal or wave influences. The work presented here documented the influence of tides and waves on the surface slope. Removal of these effects leaves the possibility of measuring discharge from water surface slope at river mouths.

Acknowledgment

The NASA Earth and Space Sciences Fellowship program funded R. Branch. Office of Naval Research Grants N00014-13-1-0084 and N00014-10-1-0932 helped fund this research. We would like to thank Dan Clark for help with the Lidar system and the USGS Oregon Water Science Center for assistance with the discharge data.

References

[1] Barbara M Hickey and Neil S Banas. "Oceanography of the US Pacific Northwest coastal ocean and estuaries with application to coastal ecology". In: *Estuaries and Coasts* 26.4 (2003), pp. 1010–1031.

[2] James PM Syvitski et al. "Predicting the terrestrial flux of sediment to the global ocean: a planetary perspective". In: *Sedimentary Geology* 162.1 (2003), pp. 5–24.

[3] David M Bjerklie et al. "Evaluating the potential for measuring river discharge from space". In: *Journal of Hydrology* 278.1 (2003), pp. 17–38.

[4] Imen Turki et al. "On the investigation of the sea-level variability in coastal zones using swot satellite mission: Example of the eastern english channel (western france)". In: *IEEE Journal of Selected Topics in Applied Earth Observations and Remote Sensing* 8.4 (2015), pp. 1564–1569.

[5] Sylvain Biancamaria, Dennis P Lettenmaier, and Tamlin M Pavelsky. "The SWOT mission and its capabilities for land hydrology". In: *Surveys in Geophysics* 37.2 (2016), p. 307.

[6] Michael Durand et al. "The surface water and ocean topography mission: Observing terrestrial surface water and oceanic submesoscale eddies". In: *Proceedings of the IEEE* 98.5 (2010), pp. 766–779.

[7] Tobias Kukulka and David A Jay. "Impacts of Columbia River discharge on salmonid habitat: 1. A nonstationary fluvial tide model". In: *Journal of Geophysical Research: Oceans* 108.C9 (2003).

[8] HR Moftakhari, DA Jay, and SA Talke. "Estimating river discharge using multiple-tide gauges distributed along a channel". In: *Journal of Geophysical Research: Oceans* 121.4 (2016), pp. 2078–2097.

[9] Gina LeFavour and Doug Alsdorf. "Water slope and discharge in the Amazon River estimated using the shuttle radar topography mission digital elevation model". In: *Geophysical Research Letters* 32.17 (2005).

[10] Austin S Hudson et al. "Remote Measurements of Tides and River Slope Using an Airborne Lidar Instrument". In: *Journal of Atmospheric and Oceanic Technology* 34.4 (2017), pp. 897–904.

[11] Benjamin D Reineman et al. "A portable airborne scanning lidar system for ocean and coastal applications". In: *Journal of Atmospheric and oceanic technology* 26.12 (2009), pp. 2626–2641.

[12] FI Gonazález. "A case study of wave–current–bathymetry interactions at the Columbia river entrance". In: *Journal of physical oceanography* 14.6 (1984), pp. 1065–1078.

[13] Jim Thomson et al. "Wave breaking turbulence at the offshore front of the Columbia River Plume". In: *Geophysical Research Letters* 41.24 (2014), pp. 8987–8993.

[14] Edwin PL Elias, Guy Gelfenbaum, and André J Van der Westhuysen. "Validation of a coupled wave-flow model in a high-energy setting: The mouth of the Columbia River". In: *Journal of Geophysical Research: Oceans* 117.C9 (2012).

[15] Çiğdem Akan et al. "On the dynamics of the Mouth of Columbia River: Results from a three-dimensional fully coupled wave-current interaction model". In: *Journal of Geophysical Research: Oceans* (2017).

[16] Ryan M McCabe, Parker MacCready, and Barbara M Hickey. "Ebb-tide dynamics and spreading of a large river plume". In: *Journal of Physical Oceanography* 39.11 (2009), pp. 2839–2856.

[17] Tuomas Kärnä and António M Baptista. "Evaluation of a long-term hindcast simulation for the Columbia River estuary". In: *Ocean Modelling* 99 (2016), pp. 1–14.

[18] Pradeep K Naik and David A Jay. "Distinguishing human and climate influences on the Columbia River: changes in mean flow and sediment transport". In: *Journal of hydrology* 404.3 (2011), pp. 259–277.
[19] Hollis M Orem. *Discharge in the lower Columbia River basin, 1928-65*. Vol. 550. US Geological Survey, 1968.
[20] Rich Pawlowicz, Bob Beardsley, and Steve Lentz. "Classical tidal harmonic analysis including error estimates in MATLAB using T_TIDE". In: *Computers & Geosciences* 28.8 (2002), pp. 929–937.
[21] Robert G Dean and Robert A Dalrymple. *Water wave mechanics for engineers and scientists*. Vol. 2. world scientific publishing Co Inc, 1991.
[22] Jim Thomson. "Wave breaking dissipation observed with "SWIFT" drifters". In: *Journal of Atmospheric and Oceanic Technology* 29.12 (2012), pp. 1866–1882.
[23] T. H. C. Herbers et al. "Observing ocean surface waves with GPS tracked buoys". In: *J. Atmos. Ocean. Tech.* 29 (2012).
[24] John C Warner et al. "Development of a Coupled Ocean-Atmosphere-Wave-Sediment Transport (COAWST) modeling system". In: *Ocean Modelling* 35.3 (2010), pp. 230–244.
[25] NOAA. *Estimation of vertical uncertainties in VDatum*. 2015. URL: https://vdatum.noaa.gov/docs/est_uncertainties.html (visited on 09/18/2017).
[26] Seth Zippel and Jim Thomson. "Surface wave breaking over sheared currents: Observations from the Mouth of the Columbia River". In: *Journal of Geophysical Research: Oceans* (2017), n/a–n/a.
[27] David A Jay, Keith Leffler, and Sebastian Degens. "Long-term evolution of Columbia River tides". In: *Journal of waterway, port, coastal, and ocean engineering* 137.4 (2010), pp. 182–191.
[28] Jeffrey Campana, Eric J. Terrill, and Tony de Paolo. "The Development of an Inversion Technique to Extract Vertical Current Profiles from X-Band Radar Observations". In: *Journal of Atmospheric and Oceanic Technology* 33.9 (2016), pp. 2015–2028. DOI: 10.1175/JTECH-D-15-0145.1. eprint: https://doi.org/10.1175/JTECH-D-15-0145.1. URL: https://doi.org/10.1175/JTECH-D-15-0145.1.

Ruth Branch received the B.S. and M.S. degrees in physics and the M.S. degree in civil engineering from the University of Washington, Seattle, WA, USA in 1998, 1999, and 2003, respectively.

She is currently a graduate student in the civil and environmental engineering department at the University of Washington. Her research interests include infrared remote sensing and relating water surface elevation changes to discharge.

Alex Horner-Devine received the B.S. degree in mechanical and aerospace engineering from Princeton University in 1995. He received the M.S. and PhD. degrees from Stanford University in 1998 and 2003 respectively.

He is currently a professor of civil and environmental engineering at the University of Washington in Seattle, WA, USA. He studies fluid mechanics at and near the river-ocean interface.

Cigdem Akan received the B.S. and M.S. degrees in ocean engineering from the Istanbul Technical University, Istanbul, Turkey in 2005 and 2007, respectively. She received her Ph.D. degree in civil engineering from the University of South Florida, Tampa, FL, USA in 2012.

She is currently a professor of civil engineering at University of North Florida in Jacksonville, FL, USA. Her research experience is primarily concerned with coastal and estuarine modeling and simulations and observations of turbulent processes in the environment.

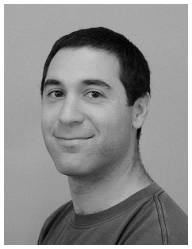

Chris Chickadel received the B.S. degree from the University of Washington, Seattle, WA, USA, in 1997, and the M.S. and Ph.D. degrees in oceanography from Oregon State University, Corvallis, OR, USA, in 2003 and 2007, respectively.

He is currently a Principal Oceanographer at the Applied Physics Laboratory at the University of Washington. His research interests include application of thermal and optical remote sensing techniques to quantify river, estuarine, and littoral fluid dynamics.

Gordon Farquharson (S'01-M'05) received the B.S.(Eng) and M.S.(Eng.) degrees from the University of Cape Town, Cape Town, South Africa, in 1996 and 1999, respectively, and the Ph.D. degree in electrical engineering from the University of Massachusetts, Amherst, in 2005, for his research on the interpretation of nearshore ocean processes.

He currently works at Capella Space designing microwave instruments for satellites.

Austin Hudson received the B.S. and M.S. degrees in civil and environmental engineering from Portland State University, Portland in 2012 and 2014 respectively. His research interests include remote sensing, etuarine turbidity maxima, sediment transport and morphodynamics.

Stefan Talke received the B.S. degree in mechanical engineering from the University of California, Berkeley in 1996. He received the M.S. and PhD. degrees from the University of California, Berkeley in 2001 and 2005 respectively.

He is currently a professor of civil and environmental engineering at Portland State University in Portland, OR, USA. His research focuses on hydrodynamic processes and sediment transport in estuaries, rivers, and the ocean using a combination of field data, analysis, and modeling.

Jim Thomson received the B.A. degree in physics from Middlebury College, Middlebury, VT, USA, in 2000 and the Ph.D. degree in oceanography and ocean engineering from the Massachusetts Institute of Technology (MIT) and Woods Hole Oceanographic Instituion (WHOI) Joint Program in 2006.

He is currently a Principal Oceanographer at the Applied Physics Laboratory, University of Washington, Seattle, WA, USA. He is also an Associate Professor of Civil and Environmental Engineering at the University of Washington. His research interests include surface waves and upper ocean turbulence.

Andrew Jessup (M'89) received the B.S. degree in engineering science from the University of Michigan, Ann Arbor, MI, USA, in 1980, the M.S.E. degree in civil engineering from the Massachusetts Institute of Technology (MIT), Cambridge, MA, USA, in 1988, and the Ph.D. degree in oceanography and ocean Engineering from the MIT and WHOI Joint Program in 1990.

He is currently the Chair of the Air-Sea Interaction and Remote Sensing Department at the Applied Physics Laboratory, University of Washington, Seattle, WA, USA. He is also a Professor of Civil and Environmental Engineering at the University of Washington. His research interests include remote sensing of river inlets and infrared techniques to study air-sea interaction.